Hindawi
Wireless Communications and Mobile Computing
Volume 2022, Article ID 1558791, 16 pages
https://doi.org/10.1155/2022/1558791

Research Article

Design and Analysis of a 5G Wideband Antenna for Wireless Body-Centric Network

Mohammad Monirujjaman Khan,[1] **H. M. Arifur Rahman**,[1] **Md. Nakib Alam Shovon**,[1] **Wajdi Alhakami**,[2] **Myriam Hadjouni**,[3] **Hela Elmannai**,[4] **and Sami Bourouis**[2]

[1]*Department of Electrical and Computer Engineering, North South University, Bashundhara, Dhaka 1229, Bangladesh*
[2]*Department of Information Technology, College of Computers and Information Technology, Taif University, P.O. Box 11099, Taif 21944, Saudi Arabia*
[3]*Department of Computer Sciences, College of Computer and Information Science, Princess Nourah bint Abdulrahman University, P.O. Box 84428, Riyadh 11671, Saudi Arabia*
[4]*Department of Information Technology, College of Computer and Information Science, Princess Nourah bint Abdulrahman University, P.O. Box 84428, Riyadh 11671, Saudi Arabia*

Correspondence should be addressed to Mohammad Monirujjaman Khan; monirkhan.qmul@gmail.com

Received 21 April 2022; Revised 5 July 2022; Accepted 7 July 2022; Published 4 August 2022

Academic Editor: Kalidoss Rajakani

A compact 5G wideband antenna for body-centric network (BCN) operating on Ka band has been presented in this paper. The design of the antenna consists of a very simple key-shaped radiator patch with a vertical slot for better impedance matching. The antenna was designed and simulated with the help of the Computer Simulation Technology (CST) Microwave Studio Suite, a well-liked and dependable electromagnetic simulation program running on Microsoft Windows. Free-space simulation produces a resonant frequency at 28 GHz, which falls under the Ka band and 5G's n257, more precisely n261. The proposed antenna has a size of $1.24\lambda \times 0.6\lambda \times 0.153\lambda$ and has a wider impedance bandwidth of more than 20 GHz. The antenna's gain and radiation efficiency are 3.87 dBi and 70%, respectively, at the resonant point. Further parametric studies reveal that the antenna can be activated in the V-band by increasing the feedline width. The antenna is proposed for the application of BCN. Therefore, a three-dimensional human torso phantom was developed virtually to test on-body performance. The on-body findings of this antenna were resimulated by positioning the antenna in close proximity to the three-layer human body model, where 22.5 dB of on-body reflection coefficient was recorded at 28 GHz. Simulated on-body gain and efficiency were 4.56 dBi and 61.33 percent, respectively. A distance-based investigation was conducted to investigate the impacts of the human body's presence by positioning the antenna at five different distances from the human torso model. The findings were compared to assess how distance affects its behaviors. The antenna's gap was kept at 6 mm for the optimum results, which included 4.83 dBi of gain with a 66 percent efficiency and a recorded RL value of about 23 dB. The on-body simulations produced very consistent results with a slight deviation after 26.5 GHz, even though the distance was varied.

1. Introduction

5G mobile communication opens up a new era in the field of telecommunication with lots of opportunities and possibilities with the availability of a wide spectrum range, lower latency, more stability, and an extremely fast data transfer rate. Telecommunication technology is evolving every day, including everything related to it. Newer generations enable more users to connect simultaneously with multiple devices, stable and efficient connections during fast-paced travel, and multiple gigabits per second data exchange. All of these require more developed transceivers that are capable of fulfilling these needs.

Since antennas are the most vital element in telecommunication technologies, researchers around the world are working relentlessly to develop more advanced antennas suitable for

newer technologies. One of the common objectives of fifth-generation communication is not only to connect all the people virtually; it is aimed at connecting everything, including devices, home appliances, gadgets, and machines. To support this goal, 5G NR (New Radio) covers a wide range of frequencies, which is divided into two sets of frequencies [1] created by the Third Generation Partnership Project, or 3GPP. The Third Generation Partnership Project is a group of standard organizations that create protocols for evolved third-generation and beyond third-generation mobile telecommunications. The first one, called Frequency Range 1, covers the frequency ranges from 410 MHz to 6 GHz, while the second, called Frequency Range 2, does the same for the bands from 24.25 GHz to 48.20 GHz. In many ways, Frequency Range 2, or mmWave 5G, outperforms Frequency Range 1, also known as sub-6 5G. As many higher frequency spectrum bands are not currently licensed, they are more popular and freely available for multipurpose applications. The FR2 spectrum is made up of six Time Division Duplexing (TDD) bands, numbered n257 to n262. Within these, n261 is a subset of the n257 band.

The 28 GHz band, which spans from 26.5 GHz to 29.5 GHz, is often referred to as 3GPP band n257. Similarly, another 3GPP frequency band ranged from 24.5 GHz to 27.5 partially overlaps the n257 band and falls on the boundary of the K band, known as the n258 band. This range is simply called "26 GHz." Another band, "n261," is in fact a subset band of n257 and ranges from 27.50 GHz to 28.25 GHz. Therefore, these "n257" and "n261" bands directly fall within the "Ka" (K above) band of microwaves, ranging from 26.5 to 40 GHz. Due to the high atmospheric absorption and attenuation, the K band is less suitable for long-range data communication. Ka band is used in a variety of applications, including police speed enforcement (n257, n259, n260, and n261), 5G mobile networks (n257, n259, n260, and n261), and communication satellites such as the NASA Kepler Mission, ACTS Gigabit Satellite Network, K-1 satellite, Space X Starlink, Iridium Next, SES O3b System, James Webb Space Telescope, and Project Ku [2–8].

In keeping pace with technological advancements, the wireless body-centric network (WBCN) is also getting equipped with newer technologies and more advanced equipment, where stronger connections, high volume, and fast-paced data exchange are becoming essential [9]. The healthcare division is a major field for body-centric networks or body-area networks. A strong, stable, low-latency connection is essential for precisely monitoring the vital physical signs, keeping the patient under real-time supervision, or syncing the bulky data between body area network (BAN) to BAN and BAN to base terminals. For the futuristic body-centric area applications, fifth-generation telecommunication could be embedded in the system for supplementary facilities like the exchange of collected physical data directly using the mobile networks. There are a lot of other places where BCN can be used, not just in healthcare facilities, like sports, entertainment, military, and defense [10–14].

For this reason, an antenna for BCN operating at the 5G frequencies could be very beneficial, which could unify wireless body area applications with conventional fifth-generation telecommunication. The goal of this research was to develop a special, effective, and compact BCN antenna that would integrate BCN operations with fifth-generation telecommunications while operating in the traditional 5G band. It is necessary for the antenna for body-centric communications to be small and less delicate to human lossy tissues. It is crucial to look into how the human body affects the antenna's performance characteristics because when an antenna is put on the human body, its performance typically varies. This inspires scientists to create an appropriate antenna for body-centric communications.

1.1. Related Existing Works. Farooq and Rather presented a 5G miniaturized antenna working at 33.5 GHz and 60.8 GHz with better on-body gain and efficiency [15]. The antenna was also tested in in-body scenarios, where it suffered performance degradation due to the human body effect. Ur-Rehman et al. proposed a triband body-centric multiple slotted antenna that showed very good off-body performance [16]. The on-body gain of the antenna was 8.3 dBi, but the efficiency was 54%. The author's another antenna for body-centric networks operated on the millimeter wave's 58 GHz, 60 GHz, and 62 GHz frequencies [17]. Shawkey and Elsheakh's dual-meander line antenna [18] for 5G BCN works on multiple bands, 58 GHz, 44 GHz, 34 GHz, and 22 GHz. According to the author, the dual-meander line structure has increased bandwidth while simultaneously increasing the number of tuning bands. Another antenna designed by Aliakbari et al., which is a circularly polarized single-fed, dual-band 5G antenna, was created with the RT duroid 5880 substrate [19]. It showed promising results for 5G mobile communication bands but was not tested for body area or body-centric networks. The antenna proposed by Huang et al. was also a dual-band millimeter-wave monopole antenna operating at 24 GHz and 60 GHz frequencies. The antenna fabrication was done with a 0.13-micron Complementary Metal Oxide Semiconductor (CMOS) technology [20]. The designed antenna by Jain et al. operates on two frequencies, 28 GHz and 38 GHz, with a notch at 33 GHz [13]. The antenna shows an omnidirectional pattern and a relatively flat gain between 3.6 and 4.4 dBi in different ranges. For next-generation wireless communication, a Hexagonal Fractal Antenna Array (HFAA) is presented in [21].

Puskely et al. have presented a wearable disk-shaped antenna for BCC where electromagnetic coupling was used instead of direct connection to the feeding pin. The antenna achieved a 5.2 dB of on-body gain with a minimum efficiency of 25% at 60 GHz [22]. Razafimahatratra et al. presented a 60 GHz antenna with a substrate integrated waveguide technique for on-body propagation channel [23], where the antenna recorded 2 dB of on-body gain while keeping 5 millimeters of gap from the antenna element and 62% efficiency. Another antenna proposed by Iqbal et al. for wearable applications operates at 24 GHz [24]. The authors used EBG and Rogers 6002 substrate with this MIMO antenna to produce on-body gain of up to 6 dB. The textile-based mmWave antenna presented by Wagih et al. operating at 26 GHz and 28 GHz exhibited an on-body peak gain of 7 dB with 40% efficiency [25]. Aside from the research reviewed above, a few more studies on 5G and mmWave antennas for body area networks [25–30] have also shown promising results. A huge wideband array antenna operating at 60 GHz for body-centric communication has been

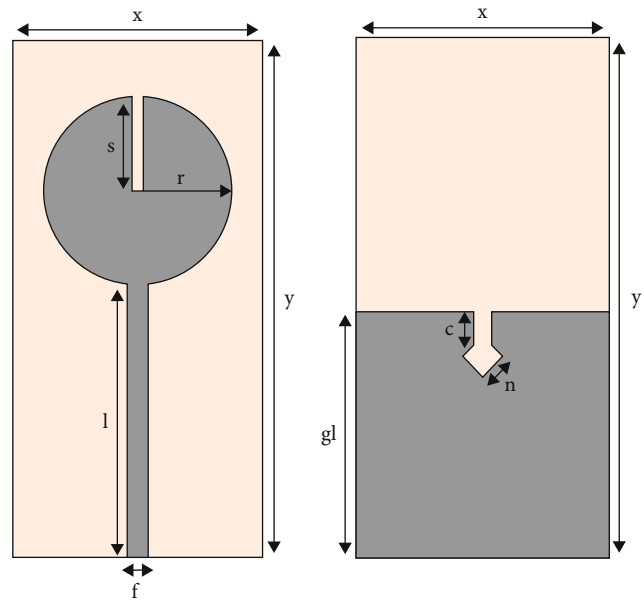

Figure 1: Antenna dimensions: (a) front and (b) back.

introduced in [31]. More than 20 GHz of bandwidth is available from the antenna [31]. The antenna shows good on-body performance at 60 GHz for different arrays. In comparison with the other state-of-the-art antennas for on-body applications, the proposed design has the simplest structure with the smallest physical dimensions, yet with a substantial amount of on-body gain and efficiency.

The goal of this study is to develop a 5G wideband antenna for a Ka band wireless body-centric network. This paper presents an antenna design operating on 28 GHz of 5G's n257 under the Ka band for body-centric network (BCN). This paper's main contribution is the design and analysis of the 5G wideband antenna that is suggested for a wireless body-centric network. The CST program was used to design the antenna, and after that, the free-space performance parameters of the antenna were examined. The on-body performance of the antenna was subsequently examined. The study's suggested antenna design is original. The antenna is incredibly small and has a huge bandwidth. When the antenna is put very close to the human body model, it performs quite well. There are antenna designs for narrowband, ultra wideband, and 60 GHz that can be applied for body-centric communications. However, very few antenna designs and comprehensive studies for body-centric networks are present.

There are eight sections in the paper. Those are as follows: introduction, antenna design, free-space simulation, parametric study, on-body simulation, distance-based study, comparison with other designs, and conclusion. Section 1 discusses 5G communication, its various bands, their applications, and establishing a relationship with body-centric networks, as well as some related recent research. Section 2 presents the antenna structure. The simulation results of the free-space and the parametric investigation are presented in Sections 3 and 4, respectively. Section 5 presents distance-based evaluations, while the on-body simulation results are described in Section 6. Section 7 compares the antenna parameters with the other BCN state-of-the-art designs. Finally, the results are used to draw a conclusion in Section 8.

Table 1: Values for antenna dimensions.

S. No.	Parameter	Value (mm)
1	x	6.44
2	y	13.30
3	l	7.02
4	s	2.45
5	r	2.45
6	f	0.56
7	gl	6.30
8	c	0.86
9	n	0.71

Table 2: Antenna materials.

Parameter	Thickness (mm)	Material	Epsilon
Ground	0.035	PEC	—
Substrate	1.57	FR4 (lossy)	4.3
Patch radiator	0.035	PEC	—

2. Antenna Design

The CST Microwave Studio Suite, a well-known electromagnetic component design and simulation program for Microsoft

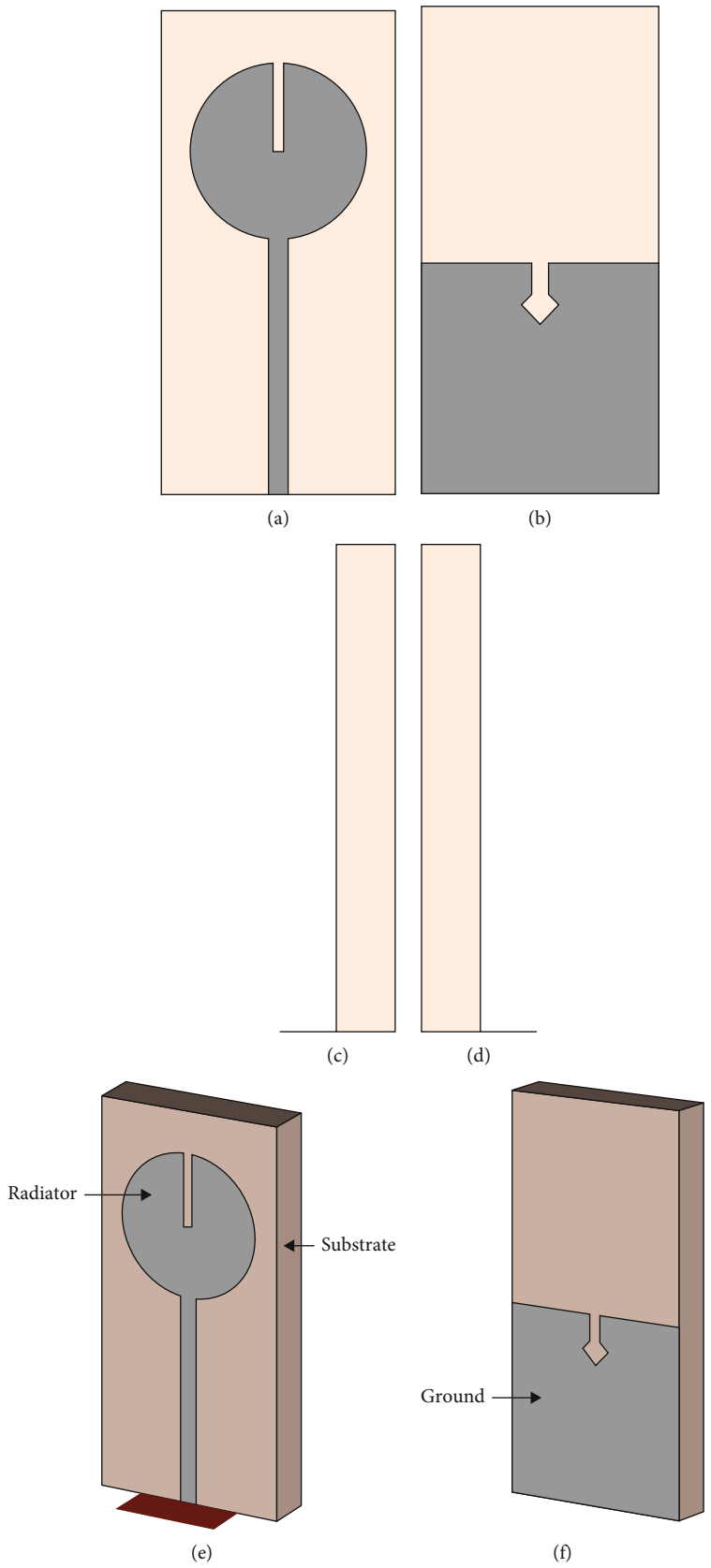

Figure 2: (a) Front view, (b) back view, (c) right view, (d) left view, (e) perspective front view, and (f) perspective back view.

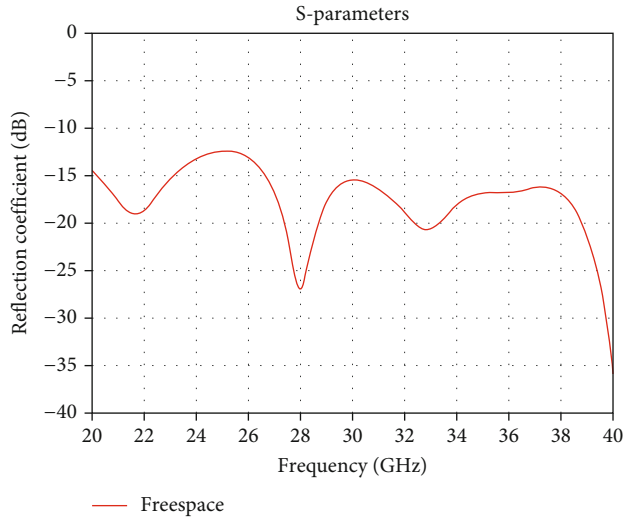

Figure 3: *S*-parameters for free space.

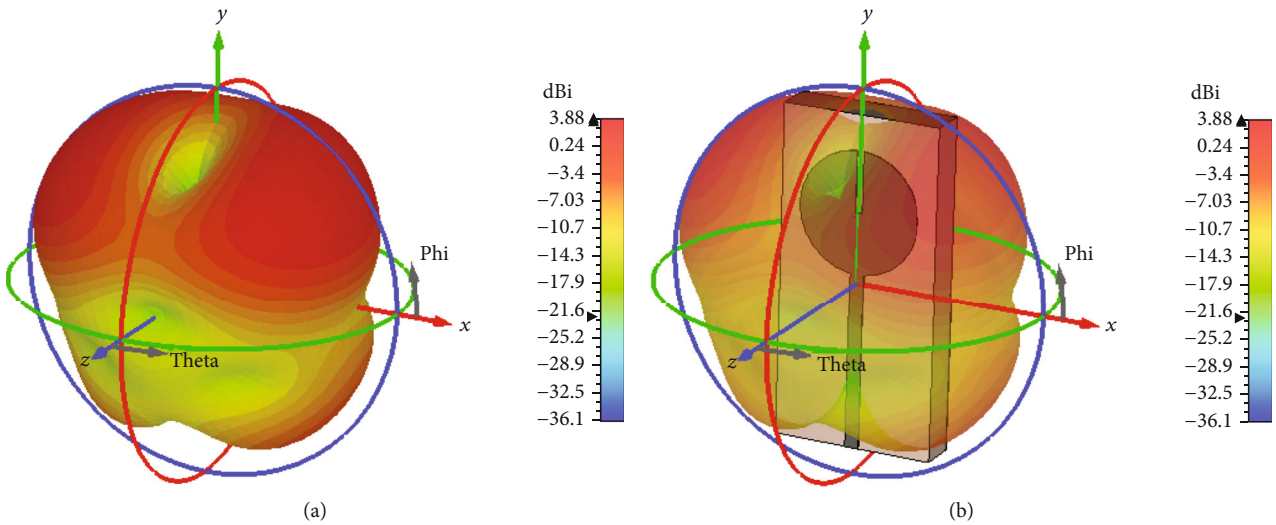

Figure 4: 3D radiation pattern in free space for 28 GHz (a) without structure and (b) with structure.

Windows, was used to develop and test the planned antenna. Figure 1 depicts the antenna's fundamental layout from both the front and back. The antenna is made with a rectangular substrate made of flame retardant fiber glass epoxy material (FR4), which was used as the substrate material. The substrate is 13.3 mm long and 6.44 mm wide. This layer is one of the three layers that stays in the middle of the other two layers, the radiator patch and the ground. The radiator is printed on top of the substrate with a circular shape with a slotted radius on top and a long narrow feedline. This has been used for good impedance matching purpose.

The narrow feedline of the patch is 7.02 mm long and 0.56 mm wide. The circular shape of the patch has a radius of 2.45 mm. A same-sized slot was cut out vertically along the feedline. Below the substrate, the adjacent layer is the ground, which covers the bottom part of the substrate. The ground dimensions are 6.44 mm × 6.30 mm. A tiny slot was created with a square shape on the bottom of it. The proposed antenna's wavelength at 28 GHz is 10.71 mm. The electrical size of this antenna with its substrate is $1.24\lambda \times 0.6\lambda \times 0.153\lambda$ (length × width × thickness).

The various antenna parameters and their related lengths are displayed in Table 1. These parameters can be matched with the front and back views of the antenna presented in Figure 1.

In Table 2 presented above, specifications of the different layers are given with their corresponding thicknesses, permittivity, and materials used to create those layers. The ground layer and the patch radiators are of the same thickness of 0.035 mm. For both layers of this design, a perfect electric conductor (PEC) material was employed. As a result, their permittivity was undefined. The substrate layer was

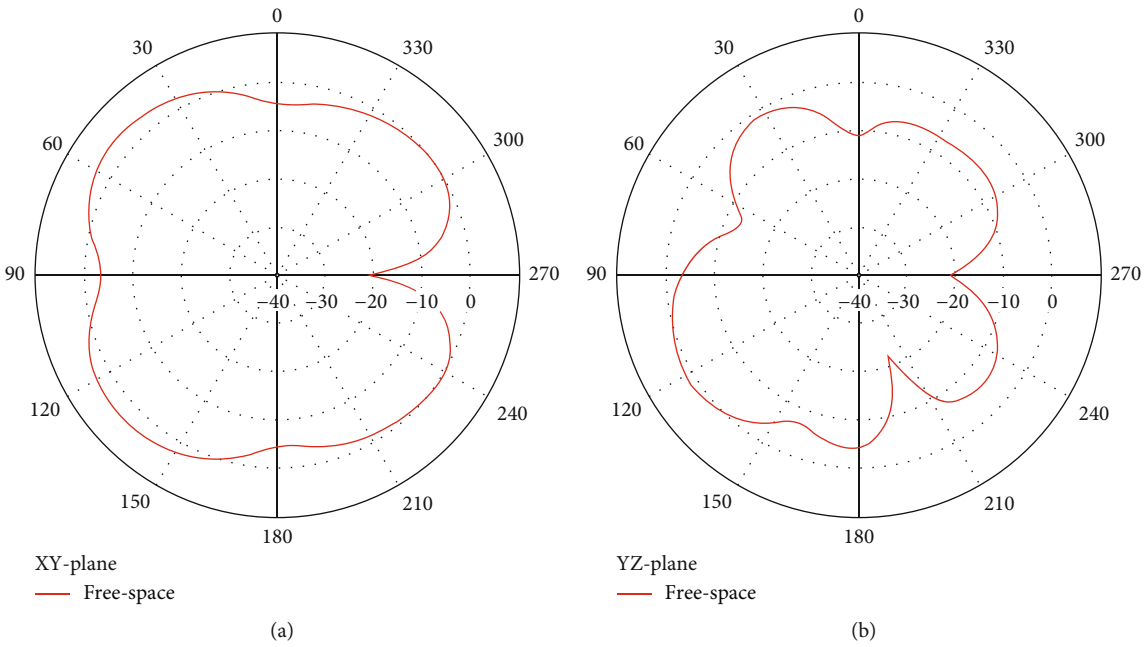

Figure 5: 2D radiation pattern in free space for 28 GHz on the (a) XY plane and (b) YZ plane.

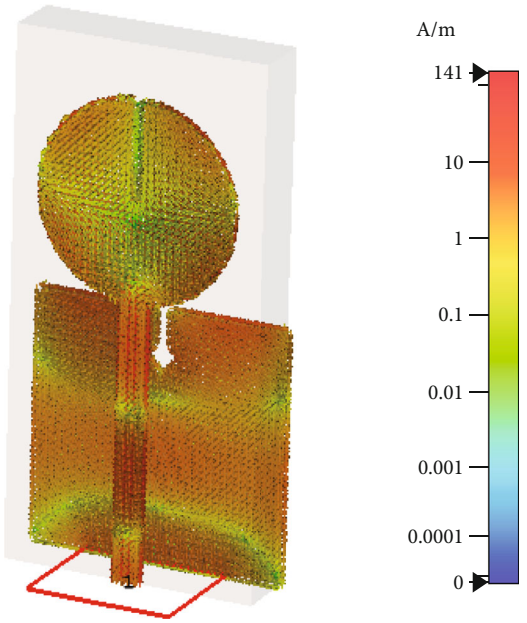

Figure 6: Surface current in free space at 28 GHz.

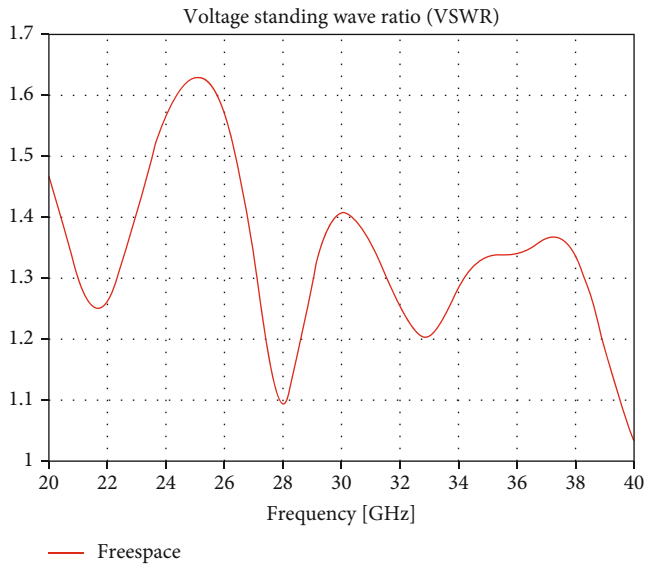

Figure 7: VSWR in free space at 28 GHz.

constructed from FR4 (lossy) material, which has a dielectric constant of 4.3 and a loss tangent of about 0.02.

In Figure 2, shown above, different views of the antenna are given. Figures 2(a) and 2(b) are the front and back views of the antenna. The antenna is viewed from the right and left in Figures 2(c) and 2(d). Figures 2(e) and 2(f) are the three-dimensional perspective views of the antenna from the front and the back. Three layers of the antenna are indicated in the last three figures.

3. Free-Space Simulations

3.1. Return Loss. The antenna was simulated in free space for frequencies between 20 and 40 GHz. The curve for the reflection coefficient is shown below.

The return loss response of the antenna over the simulated frequency range is shown in Figure 3. At 28 GHz, the resonant frequency can be found. The entire curve stayed under 10 dB of return loss, demonstrating the antenna's extremely wide impedance bandwidth. The recorded reflection coefficient at the resonant frequency is -26.96 dB. However, the much wider

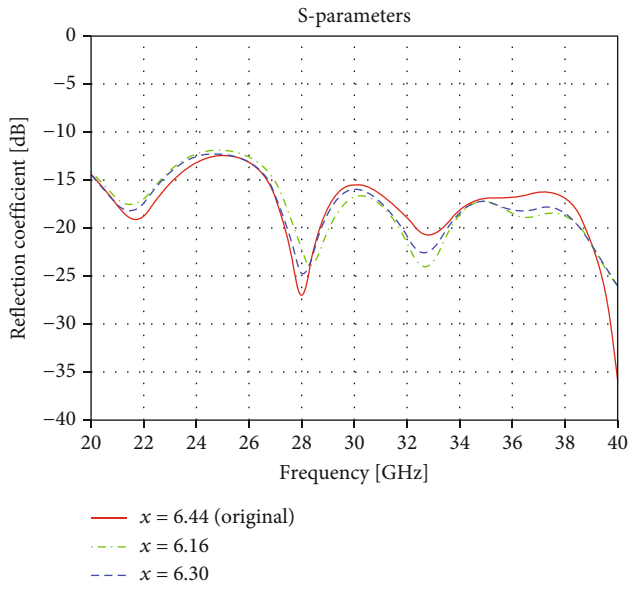

Figure 8: Comparison of S_{11} curves with different "x" values.

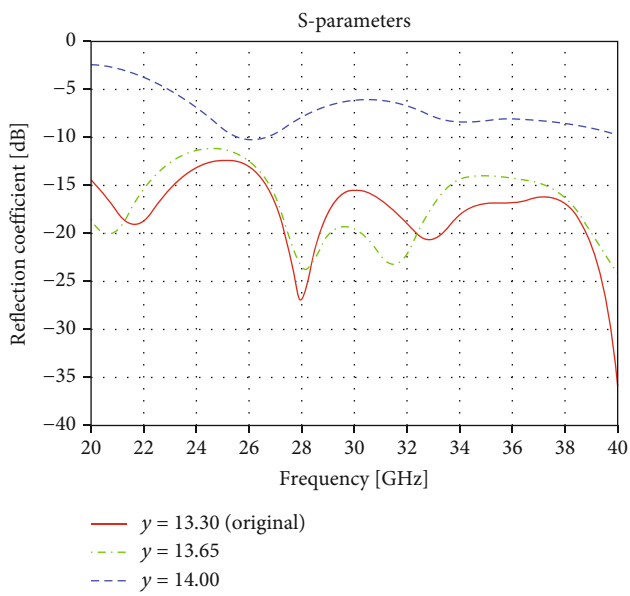

Figure 9: Comparison of S_{11} curves for different "y" values.

bandwidth could not be determined as the cut off points were outside the simulated range.

3.2. 3D Radiation Patterns. The return loss response of the antenna over the simulated frequency range is shown in Figure 3. At 28 GHz, the resonant frequency can be found. The entire curve stayed under 10 dB of return loss, demonstrating the antenna's extremely wide impedance bandwidth. Figures 4(a) and 4(b) show the 3D radiation patterns of this antenna. The antenna shows a maximum gain of 3.88 dBi in the free-space simulations. The pattern shows its maximum gain was achieved along two directions on the XY plane, in the first and the second quadrant, which is almost symmetrical along the positive Y-axis.

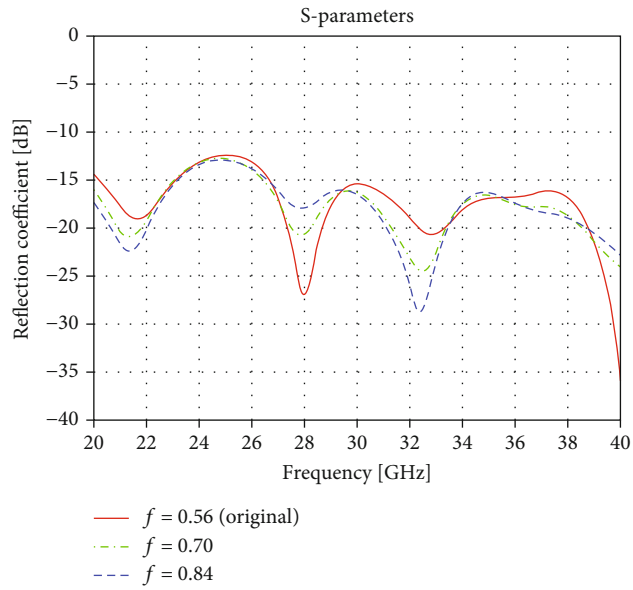

Figure 10: Comparison of S_{11} curves for different "f" values.

3.3. 2D Radiation Patterns. Two-dimensional radiation patterns at 60 GHz are shown in Figures 5(a) and 5(b), respectively, on the XY plane and the YZ plane. The antenna's radiation pattern in the XY plane indicates its main lobe orientation of 135 degrees with around 45 degrees of 3 dB angular width. Another side lobe can be seen at 70 degrees with the same angular width. The main lobe direction in the YZ plane's pattern is roughly 120 degrees. Multiple lobes at different angles make the YZ plane radiation patterns seem deformed.

3.4. Surface Current. Figure 6 illustrates how the surface current spreads when the antenna is activated using "port 1" at a 28 GHz frequency. The maximum density reached 141 amperes per meter around the radiator patch and the ground plane.

3.5. VSWR. Figure 7 displays the voltage standing wave ratio (VSWR) of the antenna within the simulated range. The VSWR value at the center frequency is slightly below 1.1, which is pretty close to the ideal value. In theory, the ideal VSWR value for an antenna is 1. This antenna in free space shows a very good VSWR value, as noticed from Figure 7, with no values above 1.65.

4. Parametric Study

After doing free-space simulations for the desired frequency range, parametric research was carried out by altering a few parameters of some of the physical sections of the antenna, redoing the simulation, and comparing the results to the primary free-space simulation results. The primary intention was to better understand the nature of the antenna and how it reacts to simple changes in the design. The parametric analysis was carried out based on changes in the relevant return loss response curve.

Table 3: Parametric study.

Parameters	Free space	$x = 6.16$	$x = 6.30$	$y = 13.65$	$y = 14.00$	$f = 0.70$	$f = 0.84$
Reflection coefficient	-26.96	-21.89	-25.18	-20.18	-19.92	-21.12	-18.06
Gain (dBi)	3.876	5.089	5.055	4.846	4.985	3.364	3.643
Radiation efficiency (%)	70.30	95.78	95.64	95.24	95.01	69.56	69.00
Bandwidth	—	—	—	—	—	—	—

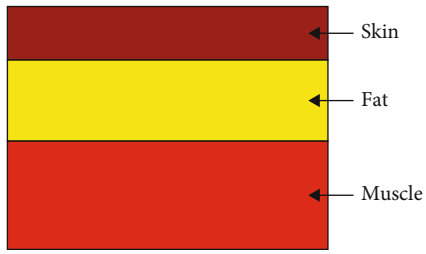

Figure 11: Torso phantom.

Table 4: Dimensions of the phantom torso [32].

Parameter	Length (mm)	Width (mm)	Thickness (mm)	Epsilon	Conductivity (S/m)
Skin	20	12	2	16.552	25.824
Fat	20	12	3	3.6985	1.6979
Muscle	20	12	4	24.44	33.609

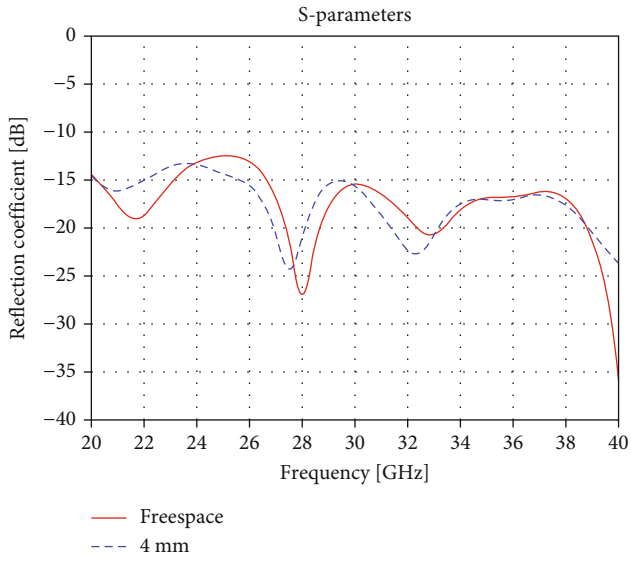

Figure 12: *S*-parameters comparison between free space and on-body.

First, the antenna dimension was modified by altering the width of the substrate, which made the antenna a little wider.

Figure 8 displays the various return loss curves for the antenna for various substrate widths. The initial antenna had a 6.44 mm width. This width was initially reduced by 0.14 mm while all other measures remained constant. The return loss curve of the antenna substrate at 6.30 mm wide, which slightly moves the resonant frequency to the right, is shown in the above figure as a blue curve. The reflection coefficient value has been increased a bit. Now, the width of the substrate has narrowed down to 6.16 mm. The green curve represents the return loss for this case. This time, the resonant frequency shifts to the right more, with an increased reflection coefficient value (-21.89 dB).

All the changes in the measurements were discarded, and the original design was restored. Now, the length of the substrate has been increased by 0.35 mm to check the effect.

In Figure 9, the red curve is the return loss response for the original design. Simulating after increasing the length by 0.35 mm shifts the whole curve to the left with its resonant point. The green curve is the S_{11} plot when the length of the substrate is 13.65 mm. At this point, the RL value increases by a tiny amount at our desired frequency of 28 GHz. At a further increment in the length by 0.35 mm, the S_{11} curve shows more losses by the blue line.

The final change was made by varying the width of the feedline. Previous changes were discarded before the new investigation. The original feed width was 0.56 mm. In Figure 10 shown above, the red curve is for the return loss of the original design. Increasing the feedline width kept the return loss curve in a very similar shape to the original but massively changed the RL values in different parts. The blue and green curves are the plots of the reflection coefficient when the feed line widths were 0.84 mm and 0.70 mm, respectively. For both the 0.84 mm and 0.7 mm wide feed lines, a new resonant frequency was formed at 32.45 GHz.

4.1. Comparison. The findings of all the parametric studies performed above are summarized in Table 3 below, where the results are compared in terms of return loss, gains, radiation efficiency, and bandwidths.

The results are compared for different parameters with each other and with the original design in Table 3. For all the modified designs, the reflection coefficient achieved for the original design in free space is the minimum. Except for this, the design with the 6.30 mm substrate width has the closest return loss value, which is -25.18 at 28 GHz. Both the radiation efficiency and the gain increase if the substrate length and width are increased. But, increasing the width of the feedline decreases both the gain and radiation efficiency compared to the primary design. It seems that the feed line measurements on the original designs produce the best results.

5. On-Body Performance Test

A radiating antenna's intrinsic characteristics are altered by the presence of a human body nearby, occasionally impairing

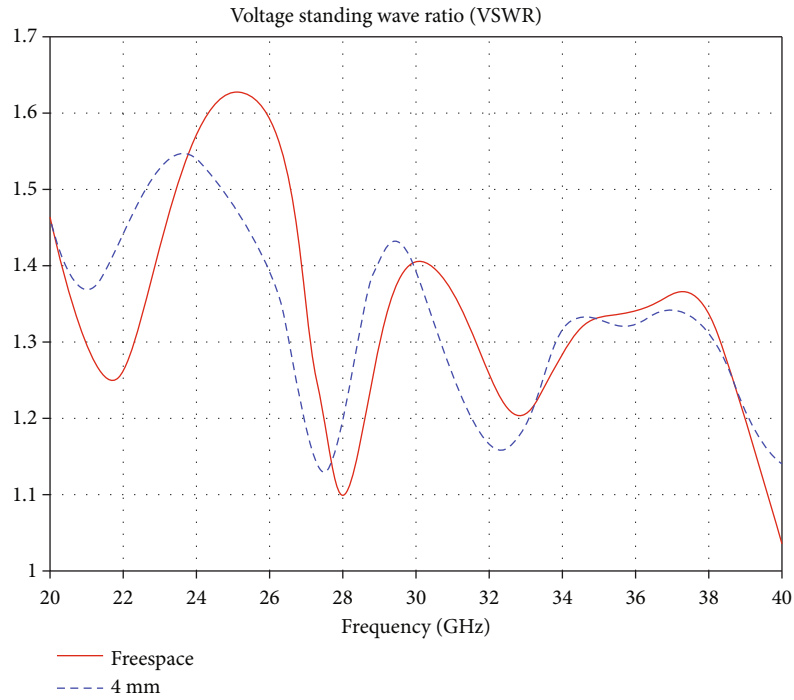

Figure 13: VSWR comparison between free space and on-body.

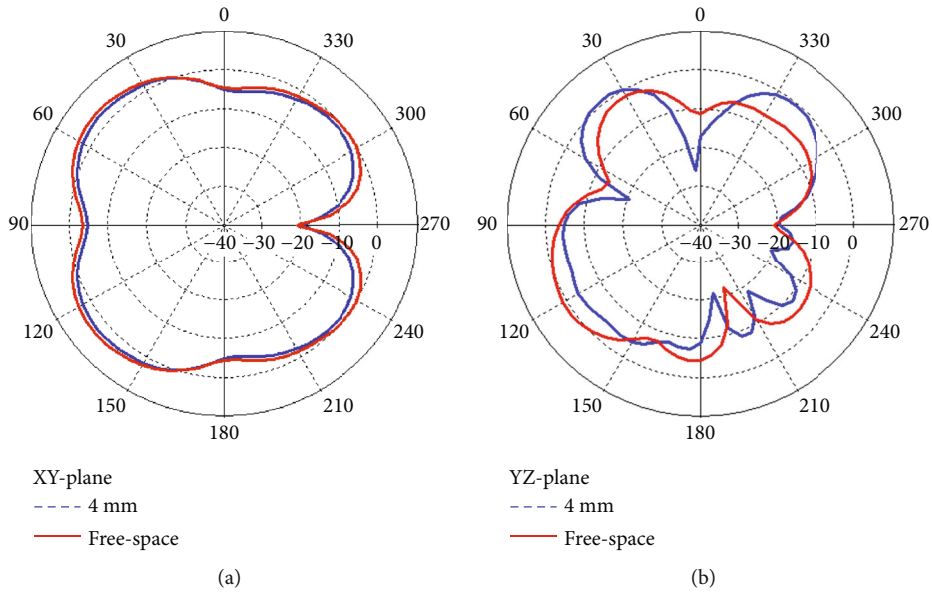

Figure 14: 2D radiation pattern comparison between free space and on-body at 4 mm (a) on the XY plane and (b) on the YZ plane.

its performance. Therefore, it becomes mandatory to check an antenna's human on-body performance before implementing it in wireless body area network operations. For this purpose, an artificial human torso phantom was created in a three-dimensional virtual environment in CST. Figure 11 shows a human torso phantom. The three outermost layers of the human body—skin, fat, and muscle—make up the fabricated torso phantom. The thicknesses of these adjacent layers were taken from the average thicknesses of the human body layers. The top layer is the skin, with 2 millimeters of thickness. Below the skin, the fat layer is a little thicker than the skin, which is 3 mm thick. The third and innermost layer is the muscle. This layer is also the thickest of the three. For the purpose of the on-body test, a 4 mm depth of the muscle layer was created and used. The key-shaped antenna was then put above the torso phantom, and its performance

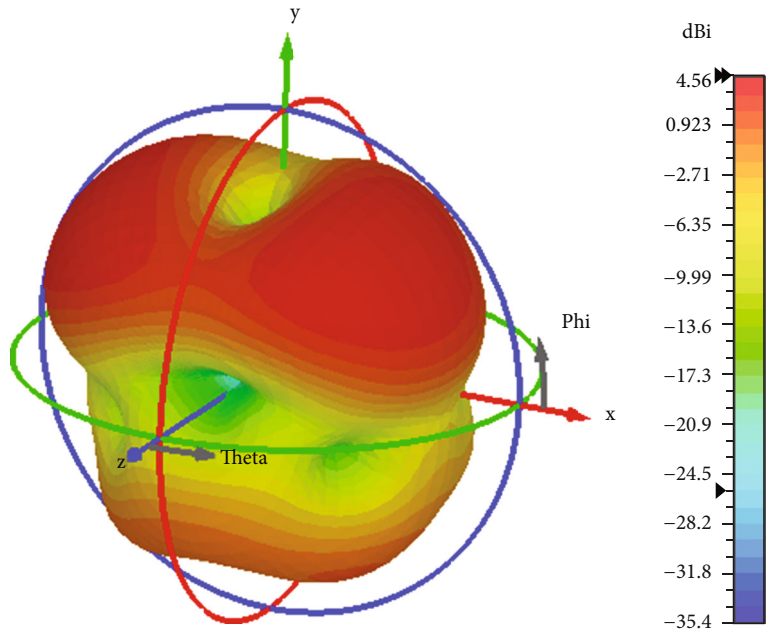

(a)

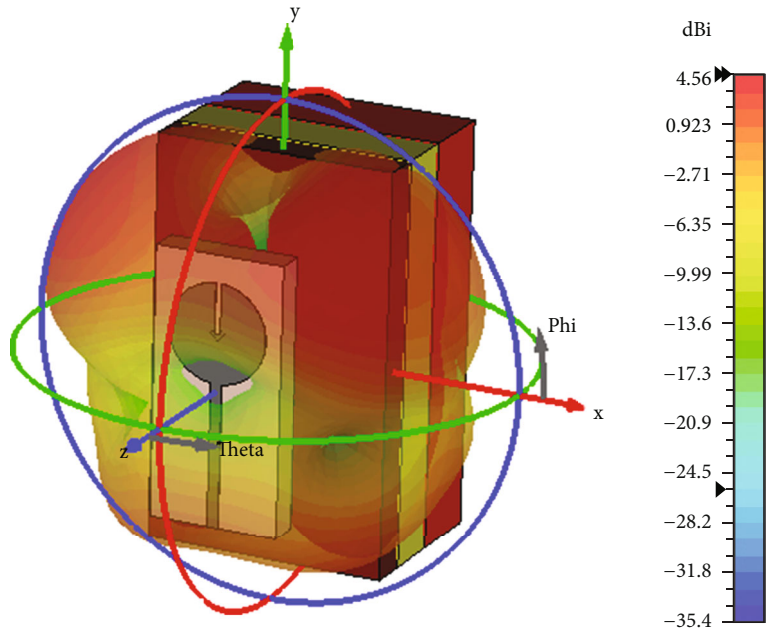

(b)

Figure 15: Continued.

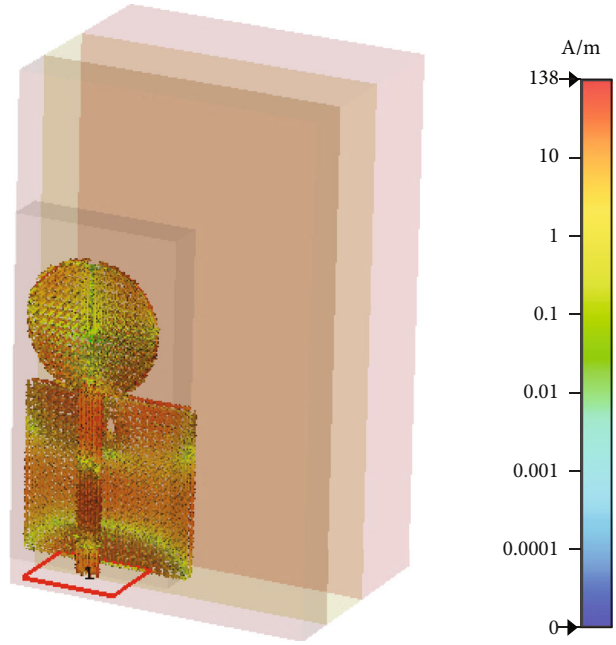

(c)

Figure 15: On-body 3D radiation patterns with 4 mm gap: (a) without structure, (b) with structure, and (c) surface current.

was tested by replicating all of the data. After that, the results were compared to those of a free-space simulation. Table 4 below shows the three layers of the torso phantom's dimensions and electromagnetic characteristics.

Specifications for the many layers of the human torso phantom are provided in Table 4 above. Table 4 lists the specs and physical dimensions of the many layers that make up the human torso phantom. All the layers have the same length and width, which is 20 mm × 12 mm. The dielectric constants of the layers are 16.552, 3.6985, and 24.44 for the skin, fat, and muscle layers. The electric conductivities are provided in siemens per meter.

5.1. On-Body Return Loss. The antenna's on-body return loss is represented on the same graph as the open space frequency response in Figure 12. The antenna was positioned 4 mm away from the phantom human torso for the general on-body simulations. Though the return loss value has degraded a little in the on-body test, the return loss value still stays below -22 dB at the center frequency. The bandwidth remained somewhat similar to the earlier result, as the whole curve remained under-10 dB.

5.2. On-Body VSWR. The antenna's voltage standing wave ratio (VSWR) curve for an on-body simulation with a 4-millimeter gap is shown in Figure 13. The VSWR value slightly increased for the on-body test performed compared to the free-space simulation but produced good results as the value is still below 1.2 at the desired frequency.

5.3. On-Body Radiation Pattern. The two-dimensional human on-body radiation patterns of the antenna in the XY and YZ planes are shown in Figure 14 above. The 2D graph in the XY plane of Figure 14(a) displays patterns that are quite similar in both the free-space and on-body simulations. A certain power loss may be seen in various directions in the radiation patterns on both planes as a result of the organic components in the human body that were positioned close to the antenna having lossy capacitive qualities. Patterns on the YZ plane given in Figure 14(b) show some changes in directivity in the on-body tests than in the free-space simulation, where the lobes are more distinguished from each other.

5.4. On-Body 3D Radiation Patterns. The three-dimensional radiation patterns of the antenna without and with the antenna for human on-body simulations are shown in Figures 15(a) and 15(b), respectively. The antenna had a 4 mm space between it and the phantom torso. The antenna's maximum gain in the on-body test was 4.56 dBi, as shown in the figure. The main lobe direction seems to be in the XY plane. Figure 15(c) shows the surface current distribution for the human on-body simulation. A maximum of 138 ampere/meter of current concentration is visible, which was distributed on the radiator patch and the ground layers.

6. Distance-Based Study

It is vital to determine the potential impact zone by positioning the antenna at various distances from the human body in order to better understand the consistency and behavior of the antenna because the presence of the human body affects how well it performs. In order to achieve this, the antenna was positioned at five different distances, ranging from 2 millimeters to 10 millimeters, each gradually rising by 2 millimeters.

The antenna was placed above the torso at varying distances, as shown in Figure 16. Separate simulations were used to analyze antenna characteristics for each distance,

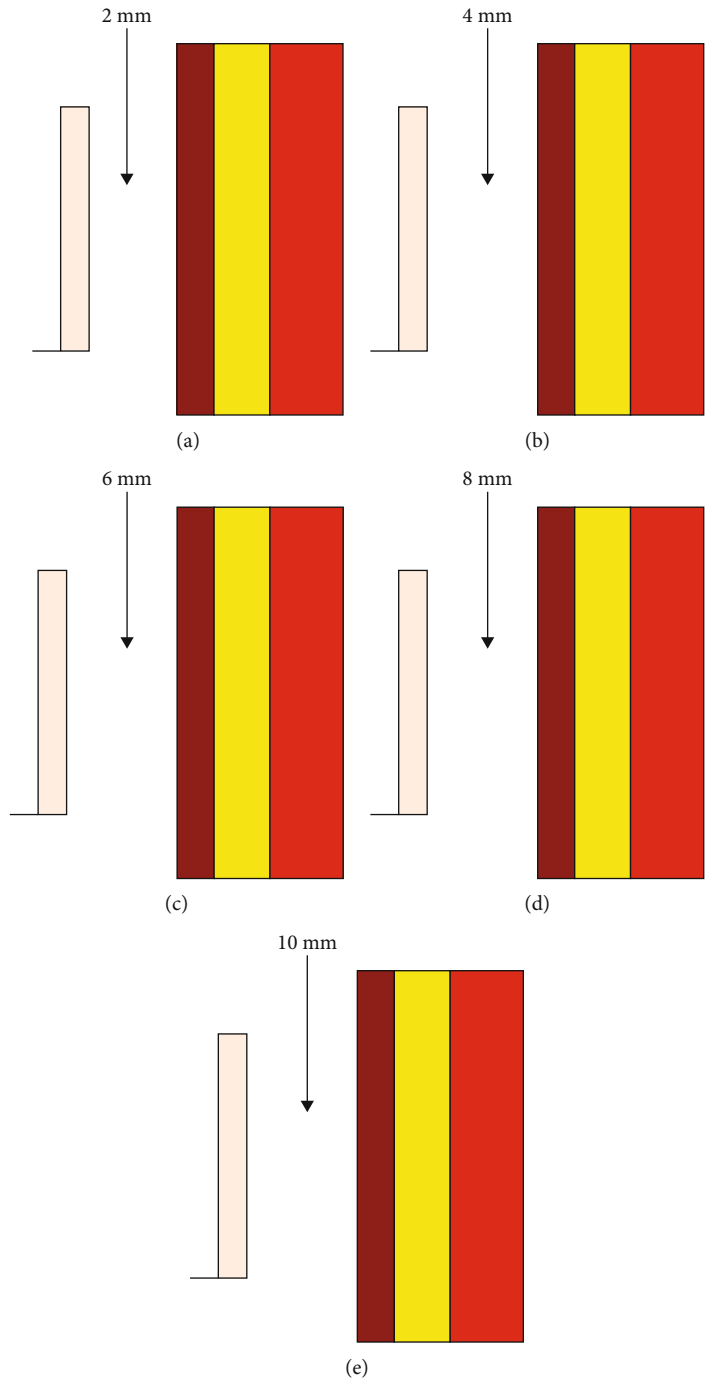

Figure 16: Views from the right for on-body antenna placements at different distances: (a) at 2 mm, (b) at 4 mm, (c) at 6 mm, (d) at 8 mm, and (e) at 10 mm.

which were then compared to each other and the previously simulated free-space data.

In Figure 17, where frequencies in gigahertz were presented on the X-axis and reflection coefficient in decibels (dB) along the Y-axis, the simulated return loss curves were shown when the antenna was situated at various distances from the human torso phantom. The red curve in the figure represents the frequency response of the antenna in free space, which had the lowest return loss at 28 GHz. For all the on-body test scenarios, the whole curve gets slightly left-shifted. The reflection coefficient fluctuated between -19.6 dB and -26 dB but never exceeded -19.5 dB. A new resonant point emerged at 34.5 GHz only for the 2 mm gap. So far, the best on-body return loss has been recorded at a 6 mm gap between the torso phantom and the antenna.

Voltage standing wave ratios oscillated between 1.1 and 1.25, which can be seen in Figure 18's curves. The distance varying curves showed consistent results with the S_{11} plotting presented in Figure 17. On-body VSWR values were found to be reasonable and much closer to unity, though the 2 mm gap

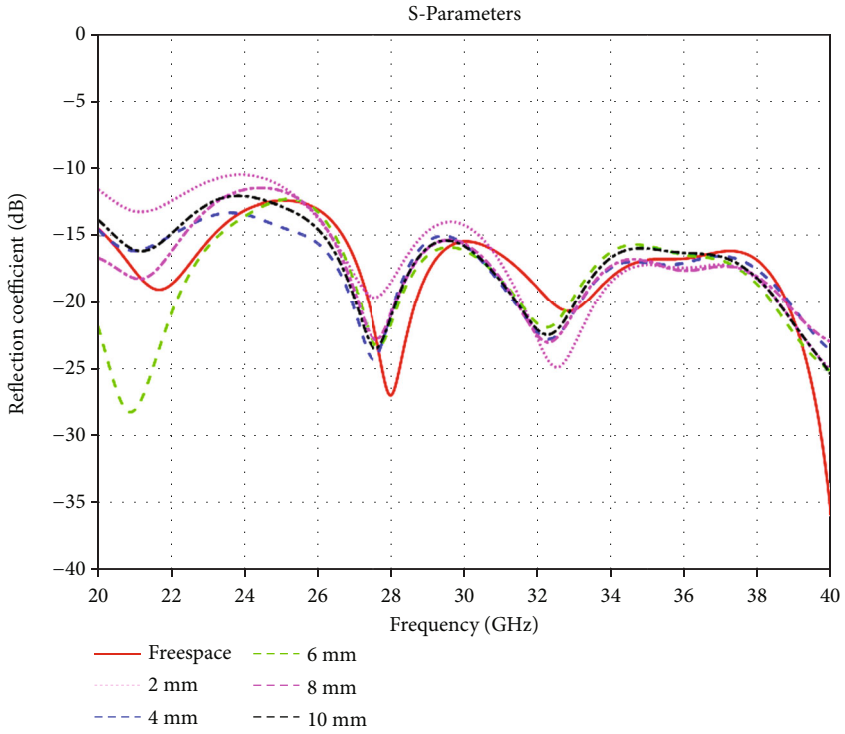

Figure 17: Comparison of reflection coefficients for different gaps between the antenna and the human body.

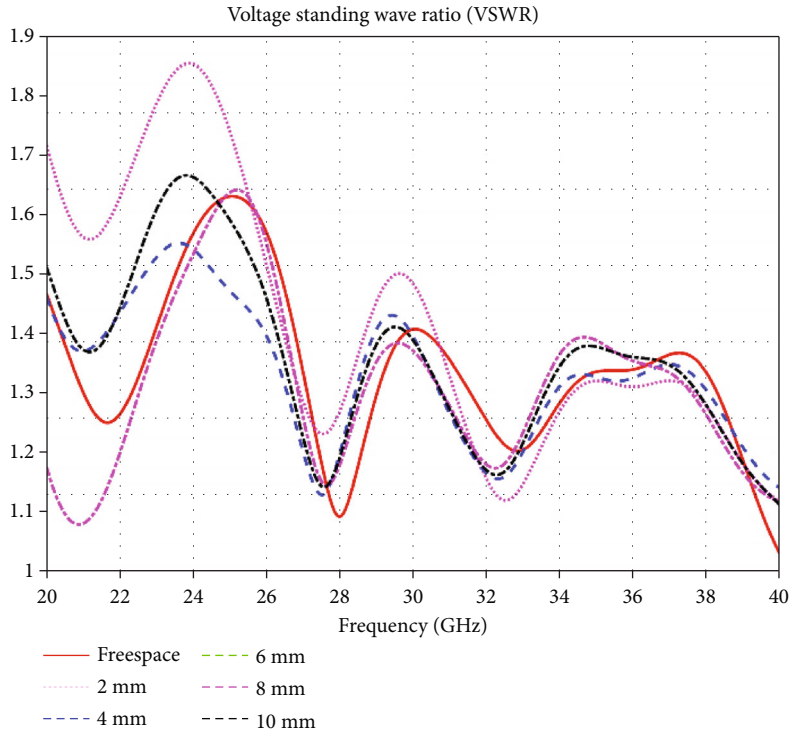

Figure 18: VSWR comparison for various distance on-body.

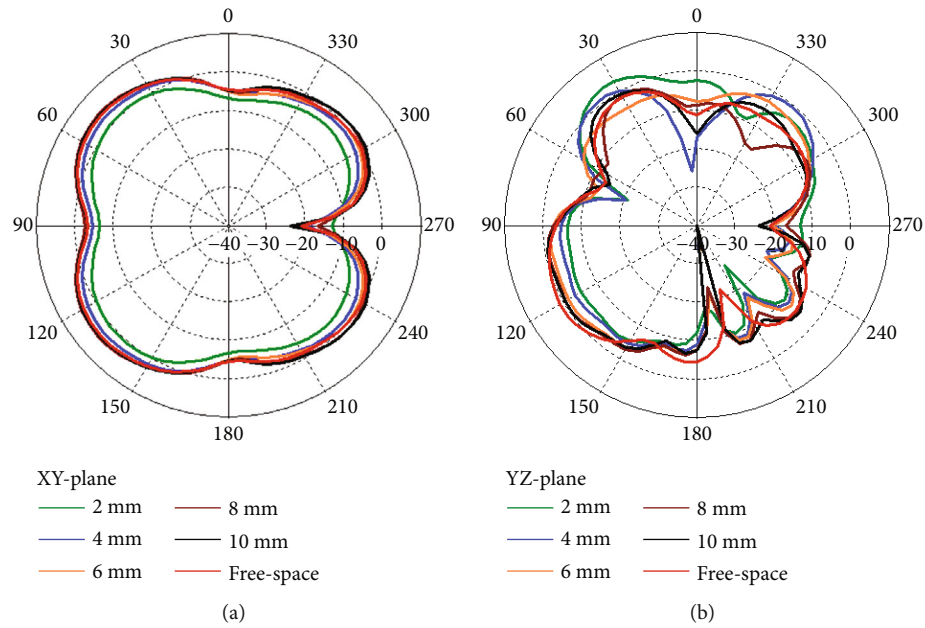

Figure 19: 2D radiation pattern comparison for various on-body distances (a) on the XY plane and (b) on the YZ plane.

Table 5: Comparison criteria and outcomes.

Parameters	Free space	On-body 2 mm	On-body 4 mm	On-body 6 mm	On-body 8 mm	On-body 10 m
Reflection coefficients	-26.96	-19.59	-22.63	-22.96	-22.40	-22.75
Gain (dBi)	3.876	4.167	4.559	4.833	4.586	4.195
Radiation efficiency (%)	70.30	50.92	61.33	65.95	68.72	69.37
Bandwidth	—	—	—	—	—	—

Table 6: Comparison with other designs.

	Physical dimension (mm)	Reflection coefficient (dB)	Gain (dB)		Efficiency (%)		Bandwidth (GHz)	Frequency (GHz)
			Free space	On-body	Free space	On-body		
Design 1 [22]	49.7 × 31 × 3.1	-22.5*	4.7	6.7	65	25	4.1	61
Design 2 [23]	24 × 17 × 0.79	Unidentified	6.6	4.4	92	62	5.8	60
Design 3 [24]	19 × 15.06 × 0.25	Unidentified	U/I	U/I	6	80.5	0.1	24
Design 4 [25]	20.27 × 9.5 × 0.46	-16, -12*	5.4, 5.5	6.2,6.6	76.9, 77.5	49, 53	2.4, 2.1	26, 28
Design 5 [proposed]	6.44 × 13.3 × 1.64	-26.96	3.876	4.833	70.30	65.95	Unidentified	28

*Approximate value.

produced the highest VSWR. The lowest VSWR values were produced at 4 mm and 6 mm distances.

In Figure 19, a two-dimensional radiation pattern on both the XY (Figure 19(a)) and YZ (Figure 19(b)) planes was plotted for all five distances. Radiation patterns on the XY plane for distance-varying on-body simulations look very consistent without any notable deviation from the free-space simulation either in the lobe directions or gain values, whereas on the YZ plane, patterns appear slightly unsettled in terms of directivity when very close to the human body, i.e., for a 2 mm gap, but the gains were fine.

Results for on-body and free space are compared in Table 5. The antenna is positioned 2, 4, 6, 8, and 10 mm distant from the torso phantom in various on-body simulations. The comparison was made with regard to reflection coefficients, gain, radiation efficiency, and bandwidth. In terms of reflection coefficients, a distance of 6 mm from the torso phantom yields the lowest on-body reflection coefficient of -22.96 dB. Except for the 2-millimeter distance, all the other simulations displayed a reflection coefficient of less than 22 dB, and the values were very close to each other. Similar phenomena were observed for both the gain and radiation efficiency results. 4.83 dB was the highest gain that was obtained when the antenna was set 6 mm away from the body model. Due to the higher conductivity and different dielectric values than those of the free space, a sudden increment of gain is observable for

on-body conditions with some degraded radiation efficiency. The radiation effectiveness is decreased when the antenna is positioned on the body because of the lossy human tissues. The gain on the human body rises as a result of the phantom's reflection. The radiation efficiency progressively increases as the antenna is positioned farther from the body. Due to the lossy tissues of the human body, when the antenna was placed on the body, the radiation efficiency on the three-layer phantom was decreased. The cutoff frequencies were found to be outside of the simulated range, while the bandwidths were found to be rather wide.

7. Comparison with Other Designs

In Table 6, a comparison of the proposed antenna design and other cutting-edge BAN/BCN designs is made. The parameters presented in Table 6 are the state-of-the-art antenna designs for wireless body-centric networks compared with the proposed antenna's results. The proposed antenna has the smallest physical dimensions compared to the other BCN antennas in the table. All the antennas presented in Table 6 [22–25] are much bigger in size in comparison with the proposed antenna in this study. The suggested antenna has an overall substrate length and breadth of 13.3 and 6.44 mm, respectively. To achieve satisfactory on-body results, design two introduced a substrate integrated waveguide (SIW), and design three employs a double element MIMO over electromagnetic band gap (EBG), whereas the simplified structural design of the proposed antenna has achieved adequate on-body gain and efficiency without implementing any complex techniques. The bandwidth was also much wider than the others, with a low reflection coefficient. This antenna shows a very large impedance bandwidth compared to other antennas presented in [22–25]. Moreover, there are quite a few BCN antennas that operate in the 5G's n257 and n261 bands, like the design presented in this paper.

8. Conclusion

A 5G wideband antenna for body-centric warless communications operating on the Ka band is designed, and the performance of the antenna is analyzed. The proposed antenna design behaved wonderfully in free-space simulations. However, it also functioned admirably on the body. The antenna also performs much more consistently in on-body simulation. The return loss in various scenarios showed stable performance of the antenna from the 26 GHz and onward frequencies, which qualifies the antenna's application in both the 3GPP's n257 and n258 bands for 5G NR FR2. However, the antenna also qualifies as functional and quite steady, especially when it is positioned more than 2 millimeters from the human body, according to the numerous on-body simulations. Placing very close to the human body hampers the antenna parameters, which is a common phenomenon. Due to the object's strong impact on the antenna's near-field distribution, detuning effects will become more noticeable at closer separation distances. Specifically, electromagnetic radiation, including the key characteristics, is strongly changed when an antenna is located close to an organic body or a living entity. This results in changes to the antenna's performance. The high conductivity value and various dielectric characteristics of human flesh are mostly responsible for this effect [33]. But, a 2-millimeter distance is very reasonable and can be maintained easily by the thickness of the wearable fabric or the hard case of the device that equips the antenna. When conducting the simulations for distance-based analysis, a 6 mm distance yields the best results. The antenna also sustained its wider bandwidth even in the on-body results. The radiation efficiency never decreased below 60%, except for the 2 mm gap. When positioned 6 mm from the human body phantom, the suggested antenna demonstrated 4.833 dBi gain and 65.95 percent radiation efficiency. The antenna has a very wide impedance bandwidth at a distance of 6 mm from the human body phantom. According to a distance-based study, a minimum 2 mm distance from the human body should be kept in order to achieve the optimum results. Both for on-body and off-body simulations, the antenna's overall performance is satisfactory. The size of this antenna can be improved in the future to operate in the 60 GHz and THz frequency ranges. Additionally, for better comprehension, a made-up model of the antenna can be tested in real-world circumstances in both free-space and human on-body scenarios.

Data Availability

The data used to support the findings of this study are freely available at http://niremf.ifac.cnr.it/tissprop/.

Conflicts of Interest

The authors would like to confirm that there are no conflicts of interest regarding the study.

Acknowledgments

The authors would like to thank Princess Nourah bint Abdulrahman University Researchers Supporting Project number (PNURSP2022R193), Princess Nourah bint Abdulrahman University, Riyadh, Saudi Arabia. The authors would like to thank also Researchers Supporting Project number (TURSP-2020/107), Taif University, Taif, Saudi Arabia.

References

[1] C. Craven, *What is the 5G spectrum? Definition*, bysdxcentral, 2020, http://www.sdxcentral.com/5g/definitions/what-is-5g-spectrum/.

[2] R. wars, *upping the ante Car and Driver*, vol. 38, no. 4, p. 153, 1992.

[3] "Kepler (spacecraft)" JPL Horizons On-Line Ephemeris System, *NASA/JPL*, 2018.

[4] A. Nyirady, *Kacific reveals plans for second satellite*, Via Satellite, 2020, http://www.satellitetoday.com/launch/2020/10/30/kacific-reveals-plans-for-second-satellite/.

[5] R. J. Acosta, R. Bauer, R. J. Krawczyk, R. C. Reinhart, M. J. Zernic, and F. Gargione, "Advanced Communications Technology Satellite (ACTS): four-year system performance," *IEEE Journal on Selected Areas in Communications*, vol. 17, no. 2, pp. 193–203, 1999.

[6] C. Henry, "Space X seeks FCC permission for operating all first-gen Starlink in lower orbit," 2020, http://spacenews.com/spacex-seeks-fcc-permission-for-operating-all-first-gen-starlink-in-lower-orbit/.

[7] E. Howell, *James Webb Space Telescope User Documentation - JWST Communications Subsystem Space Terlescope Science Institute*, 2022, https://www.space.com/21925-james-webb-space-telescope-jwst.html.

[8] J. Foust, *Amazon unveils flat-panel customer terminal for Kuiper constellation*, Space News, 2020, https://spacenews.com/amazon-unveils-flat-panel-customer-terminal-for-kuiper-constellation/.

[9] A. Ahmed, H. A. Rahman, and M. M. Khan, "Design and analysis of a compact wideband V-band and W-band antenna for healthcare applications," in *The 12th Annual Computing and Communication Workshop and Conference (CCWC)*, USA, January 2022.

[10] V. Mani, P. Manickam, Y. Alotaibi, S. Alghamdi, and O. I. Khalaf, "Hyperledger healthchain: patient-centric IPFS-based storage of health records," *Electronics*, vol. 10, no. 23, p. 3003, 2021.

[11] S. Sengan, O. I. Khalaf, G. R. Rao, D. K. Sharma, K. Amarendra, and A. A. Hamad, "Security-aware routing on wireless communication for E-health records monitoring using machine learning," *International Journal of Reliable and Quality E-Healthcare (IJRQEH)*, vol. 11, no. 3, pp. 1–10, 2022.

[12] S. Sengan, O. I. Khalaf, S. Priyadarsini, D. K. Sharma, K. Amarendra, and A. A. Hamad, "Smart healthcare security device on medical IoT using Raspberry Pi," *International Journal of Reliable and Quality E-Healthcare (IJRQEH)*, vol. 11, no. 3, pp. 1–11, 2022.

[13] A. Jain, R. K. Dwivedi, H. Alshazly, A. Kumar, S. Bourouis, and M. Kaur, "Design and simulation of ring network-on-chip for different configured nodes," *Computers, Materials & Continua*, vol. 71, no. 2, pp. 4085–4100, 2022.

[14] C. A. Tavera, J. H. Ortiz, O. I. Khalaf, D. F. Saavedra, and T. H. Aldhyani, "Wearable wireless body area networks for medical applications," *Computational and Mathematical Methods in Medicine*, vol. 2021, Article ID 5574376, 9 pages, 2021.

[15] U. Farooq and G. M. Rather, "A miniaturised Ka/V dual band millimeter wave antenna for 5G body centric network applications," *Alexandria Engineering Journal*, vol. 61, no. 10, pp. 8089–8096, 2022.

[16] M. Ur-Rehman, M. Adekanye, and H. T. Chattha, "Tri-band millimetre-wave antenna for body-centric networks," *Nano Communication Networks*, vol. 18, pp. 72–81, 2018.

[17] M. Ur-Rehman, N. A. Malik, X. Yang, Q. H. Abbasi, Z. Zhang, and N. Zhao, "A low profile antenna for millimeter-wave body-centric applications," *IEEE Transactions on Antennas and Propagation*, vol. 65, no. 12, pp. 6329–6337, 2017.

[18] H. Shawkey and D. Elsheakh, "Multiband dual-meander line antenna for body-centric networks' biomedical applications by using UMC 180 nm," *Electronics*, vol. 9, no. 9, p. 1350, 2020.

[19] H. Aliakbari, A. Abdipour, R. Mirzavand, A. Costanzo, and P. Mousavi, "A single feed dual-band circularly polarized millimeter-wave antenna for 5G communication," in *2016 10th European conference on antennas and propagation (EuCAP)*, Davos, Switzerland, 2016.

[20] J. H. Huang, J.-W. Wu, Y.-L. Chiou, and C. Jou, "A 24/60GHz dual-band millimeter-wave on-chip monopole antenna fabricated with a 0.13-mu m CMOS technology," in *2009 IEEE International Workshop on Antenna Technology*, Santa Monica, Canada, 2009.

[21] M. M. Khan, J. Hossain, K. Islam et al., "Design and study of a mm wave wearable textile based compact antenna for healthcare application," *International Journal of Antennas and Propagation*, vol. 2021, Article ID 6506128, 17 pages, 2021.

[22] J. Puskely, M. Pokorny, J. Lacik, and Z. Raida, "Wearable disc-like antenna for body-centric communications at 61 GHz," *IEEE Antennas and Wireless Propagation Letters*, vol. 14, pp. 1490–1493, 2015.

[23] S. Razafimahatratra, J. Sarrazin, A. Benlarbi-Delai et al., "On-body propagation characterization with an H-plane substrate integrated waveguide (SIW) horn antenna at 60 GHz," in *2015 European Microwave Conference (EuMC)*, Paris, France, 2015.

[24] A. Iqbal, A. Basir, A. Smida et al., "Electromagnetic bandgap backed millimeter-wave MIMO antenna for wearable applications," *IEEE Access*, vol. 7, pp. 111135–111144, 2019.

[25] M. Wagih, A. S. Weddell, and S. Beeby, "Millimeter-wave textile antenna for on-body RF energy harvesting in future 5G networks," in *2019 IEEE Wireless Power Transfer Conference (WPTC)*, pp. 245–248, London, UK, 2019.

[26] N. Chahat, M. Zhadobov, S. A. Muhammad, L. L. Coq, and R. Sauleau, "60-GHz textile antenna array for body-centric communications," *IEEE Transactions on Antennas and Propagation*, vol. 61, no. 4, pp. 1816–1824, 2013.

[27] N. Ashraf, O. Haraz, M. A. Ashraf, and S. Alshebeili, "28/38-GHz dual-band millimeter wave SIW array antenna with EBG structures for 5G applications," in *2015 International Conference on Information and Communication Technology Research (IC-TRC)*, Abu Dhabi, United Arab Emirates, 2015.

[28] H. M. Rahman, M. M. Khan, M. Baz, M. Masud, and M. A. AlZain, "Novel compact design and investigation of a super wideband millimeter wave antenna for body-centric communications," *International Journal of Antennas and Propagation*, vol. 2021, Article ID 8725263, 15 pages, 2021.

[29] M. M. Khan, K. Islam, A. Shovon, M. Nakib, M. Baz, and M. Masud, "Design of a novel 60 GHz millimeter wave Q-slot antenna for body-centric communications," *International Journal of Antennas and Propagation*, vol. 2021, Article ID 9795959, 12 pages, 2021.

[30] O. O. Wikiman, O. Idowu-Bismark, O. Ilesanmi, S. Thomas, and D. C. Bala, "PIFA antenna design for mmWave body centric 5G communication applications," *International Journal of Electronics and Communication Engineering*, vol. 6, no. 3, pp. 6–10, 2019.

[31] A. G. Alharbi, M. M. Khan, K. Islam et al., "Comparative analysis of a super-wideband millimeter wave array antenna for body-centric communications," *International Journal of Antennas and Propagation*, vol. 2022, Article ID 6963284, 21 pages, 2022.

[32] Italian National Research Council, *Dielectric properties of body tissues in the frequency range 10 Hz to 100 GHz*, Italian National Research Council, Rome, Italy, 2021, http://niremf.ifac.cnr.it/tissprop/.

[33] N. H. Abd Rahman, Y. Yamada, and M. S. Amin Nordin, "Analysis on the effects of the human body on the performance of electro-textile antennas for wearable monitoring and tracking application," *Materials (Basel)*, vol. 12, no. 10, p. 1636, 2019.